Image Anal Stereol 2002;21:183-189
Original Research Paper

SEPARATION OF THE INTER- AND INTRA-PARTICLE POROSITY IN IMAGES OF POWDER COMPACTS

JACQUES LACAZE, ALEXIS ARNAL, JEAN-LUC DUPUY AND DOMINIQUE POQUILLON
CIRIMAT, ENSIACET, UMR INPT/UPS/CNRS 5085, 31077 Toulouse cedex 4, France
e-mail: Jacques.Lacaze@ensiacet.fr
(Accepted 26 August, 2002)

ABSTRACT

Powder metallurgy is a highly developed and cheap method of manufacturing reliable materials, either metallic, ceramic or composite. This process was used to make green compacts of iron powders with a high porosity level. This study is part of a project aimed at describing the relationships between mechanical properties and morphological features of such compacts, with particular attention paid to the shape of the grains and the compaction pressure. In this report, a method is proposed to separate the intra grain porosity from the cavities located between particles. The approach is based on the covariogram of images obtained from the surface of the compacts by means of a laser roughometer. To achieve this separation, a model of the structure is proposed which assumes that the distributions of the grains and of the intra-particle cavities are random and independent. Each distribution is characterized by two parameters. A satisfactory agreement is obtained between experimental and calculated covariograms after identification of these parameters.

Keywords: compaction, covariogram, iron powder, morphology, two-fold distribution.

INTRODUCTION

This work is part of a study aimed at characterizing the relationship between microstructural features and mechanical properties of partly densified compacts. Compacts are made from iron powders obtained in two steps (Carles *et al*., 1999): i) precipitation from an oxalate precursor of small lenticular particles (length 5 to 10 μm, cross size 1 to 3 μm) as illustrated in Fig. 1a; and ii) reduction under hydrogen of the product to give grains about 15 μm in diameter, see Fig. 1b. These grains have an overall rounded shape but are agglomerate of the initial particles and thus contain internal pores. The surface of the grains is not smooth, and these irregularities are expected to help improving the mechanical properties of the compacts (Poquillon *et al*., 2002). Usual evaluation of the surface roughness of the compacts did not show any feature which could be related to the compaction pressure. It was thus attempted to use the maps of the relative height as images to be analysed by standard image analysis procedures. Results obtained for one given compaction pressure are detailed in this report.

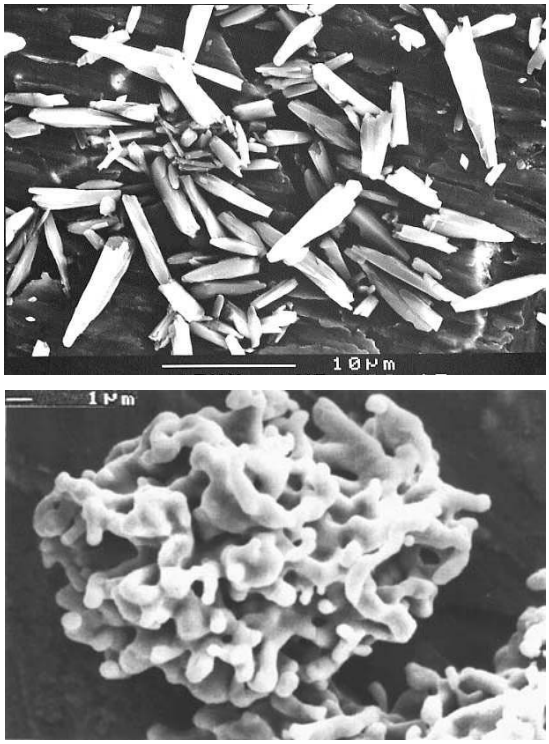

Fig. 1. *Scanning electron micrographs of the oxalate precursors (a) and of one iron powder grain (b).*

MATERIAL AND EXPERIMENTAL DETAILS

As part of a wider study dealing with the compaction process, small circular pellets 10 mm in diameter were prepared. The present investigation was carried out on a specimen compacted under a final pressure of 750 MPa. Its relative density was estimated to be about 0.8. The surface of the compact was characterized by a laser roughometer from ZYGO Corporation (Middlefield, Connecticut, USA). This apparatus has a horizontal resolution better than 1 μm and a vertical resolution better than 1 nm. Along one radius of the compact, 30 joining fields 0.176 mm long and 0.132 mm large were implemented. In each field, $N = 320 \times 240$ measurement points were performed by the roughometer, i.e. digitized maps could be drawn which have a pixel size of $0.55 \times 0.55\ \mu m^2$. The maps of the measured height showed that the surface is essentially flat with well defined holes (pores). For image analysis, the data files were used to get grey tone images to be processed with the Aphelion software (ADCIS, Caen, France). Fig. 2 shows such images corresponding to various locations along the radius. Due to the flattness of the surface, these images are much alike binary images. The fields in Fig. 2 are numbered according to their position along the radius, with field 1 close to the outer surface of the pastille. Field 1 shows a high porosity level in close relation to the distance to the outer surface. In fields 2, 4, 5, 16 and 28, large rounded holes were noted as the one seen in the image of field 5 in Fig. 2. Such holes are thought be related to the pulling out of a powder grain after compaction.

RESULTS

In Fig. 3 is plotted the evolution of the surface fraction of porosity for the 30 fields as measured by image analysis. This plot shows that apart a small heterogeneity of the compact close to the external surface, on a depth smaller than 1 mm (fields 1 to 4), most of the material appears quite homogeneously densified. Also, apart for field 1, the distribution of the porosity shows quite similar features all along the radius of the compact. Small pores appear more or less evenly distributed, but large pores are also observed which may be related to voids remaining between the grains because the compaction process has not been pursued to its end. The observation of the images in Fig. 2, in particular those of fields 10

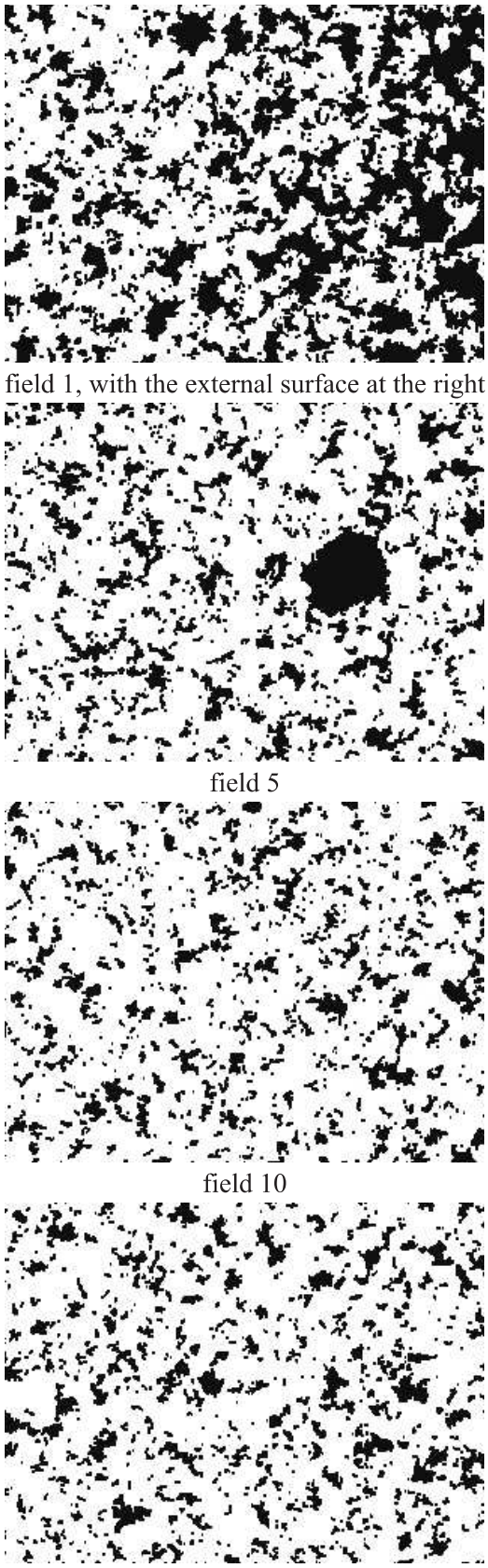

Fig. 2. *Examples of images obtained from the roughometer data file for various locations along the radius of the pellet.*

and 20, suggests that the distribution of pores could be twofold, with large elongated pores on the one hand and small pores on the other hand. It should be emphasized that, because the images were obtained from the surface of the compacts, it is very unlikely that small pores could be the visible part of large ones. When attempting to separate these two types of pores by a size criterion, it appeared that the distribution is however much more continuous than conceived at first glance. This is illustrated by the area distribution after erosion and opening with a linear structuring element parallel to the long axis of the images. The average curves obtained from all images but those close to the outer surface (1 to 4) and those with pulled out grains (5, 16 and 28) are presented in Fig. 4. It is seen that the distributions are smooth, with no sharp arrests which could be related to a characteristic size separating intra-grain from inter-grain particles.

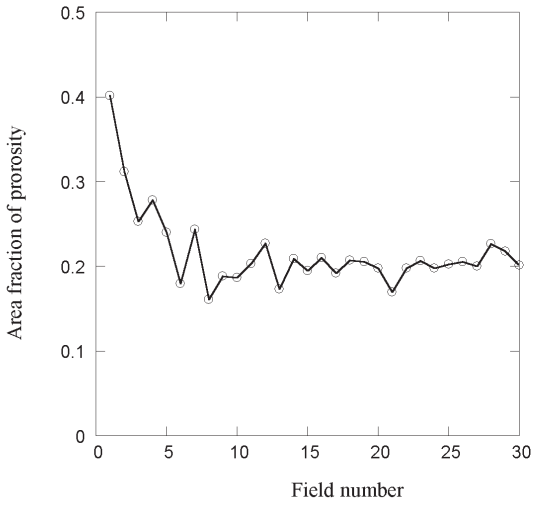

Fig. 3. *Evolution of the area fraction of porosity along a radius of the pellet.*

In view of the above result, attempt was made to use the covariogram which contains information from both the size and space distribution of the features of the images (Coster and Chermant, 1989). The covariogram of a set X, $C_X(h)$, is easily related to the auto-correlation function used by Özkan and Briscoe (1996) to study the surface topography of compacts of spheroidal alumina powder. It is defined as $C_X(h) = E\{k(x)\cdot k(x+h)\}$, where k(x) is the space function of set X and h a translation vector. The so-called local covariogram is thus obtained as the area fraction of the intersection of the initial image and the image shifted by h. In practice, h was chosen parallel to the long direction of the images and its length equal to an integral number of pixels of size $\Delta x = 0.55$ µm.

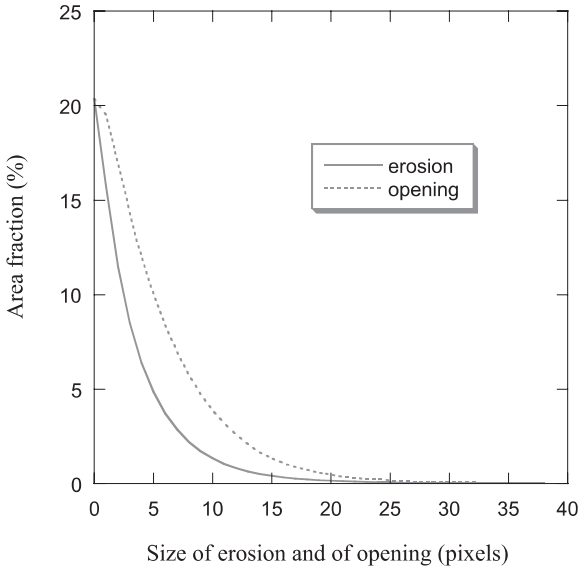

Fig. 4. *Average area distribution of the pores obtained by linear erosion and linear opening of increasing size.*

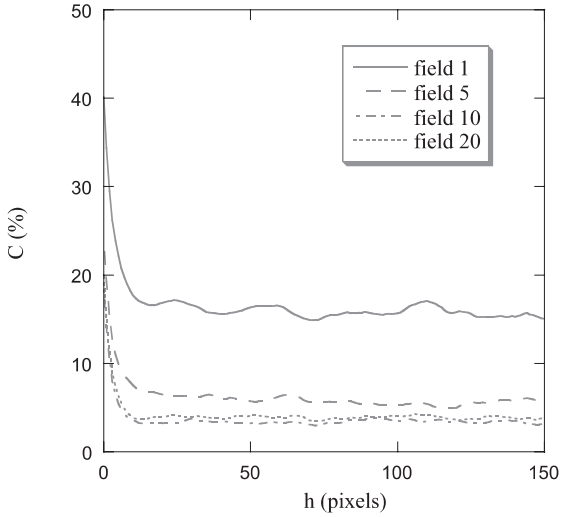

Fig. 5. *Covariogram C(h) versus h (number of pixels) for the images of the fields 1, 5, 10 and 20.*

Fig. 5 shows the curves obtained for fields 1, 5, 10 and 20 (see Fig. 2). The value of the covariance at the origin, $C_X(0)$, is the porosity fraction V_V, while the value at large h should be equal to $(V_V)^2$ if the pores are evenly distributed and if no higher order structure exists. It is seen that all four curves show the same trends at increasing value of h, a strong decrease within the first steps and then more or less periodic slight oscillation around a value close to the corresponding $(V_V)^2$ value. These oscillations are clearly visible only in the case of field 1, they could be related to the average distance between the large pores, or equivalently to the average diameter of the grains, i.e., 25 to 30 pixels or 13 to 16 µm. When

averaging the covariograms for the fields 6 to 30, disregarding fields 16 and 28, it was observed that the amplitude of the oscillations decreased. Assuming that the structure is actually homogeneous, as indicated by the stability of the porosity fraction, this means that these oscillations do not characterise any ordering of the structure but are due to the limited number of powder grains observed in each field. Moreover, the stability of the covariance at large h values may be seen as an indication that pores are randomly distributed. The characteristics of the experimental covariograms suggested to attempt to model the structure by means of boolean sets as described below.

MODELLING

Modelling was performed following the theoretical developments described by Jeulin (1979). For modelling purpose, porosity is considered as the union of cavities located within the powder grains, denoted set A in the following, and between the grains. This latter porosity constitutes the complementary set B^c of the set B of the grains without internal cavities. One thus has $X = A \cup B^c$. The covariogram of X can not be expressed directly from those of A and B^c. However, if the sets A and B are independent, the covariogram of $X^c = A^c \cap (B^c)^c$ is given as:

$$C_{X^c}(h) = C_{A^c}(h) \cdot C_{(B^c)^c}(h). \quad (1)$$

Also, if set B is isotropic, one may express $C_{(B^c)^c}(h)$ as:

$$C_{(B^c)^c}(h) = 1 - 2.C_{B^c}(0) + C_{B^c}(h). \quad (2)$$

Both the grains without internal voids and the intra-grain pores are considered to result from a random distribution (following Poisson's law) of individual objects. The covariograms $C_{A^c}(h)$ and $C_{B^c}(h)$ are given by:

$$C_{A^c}(h) = (1-q_A)^2 \cdot \exp\{\theta_A \cdot K_{A'}(h)\},$$

and
$$C_{B^c}(h) = (1-q_B)^2 \cdot \exp\{\theta_B \cdot K_{B'}(h)\}, \quad (3)$$

where q_A and q_B are the volume fraction of the intra-grain pores and of the grains respectively, θ_A and θ_B the number density (in volume) of them. $K_{A'}(h)$ and $K_{B'}(h)$ are the geometric covariograms of the average intra-grain pore A' and powder grain B' respectively. These average individual features will be described as spheres of radius a for the intra-grain pore A' and b for the grain B'. One has:

$$K_{A'}(h) = (a^3 - 1.5ha^2 + 0.5h^3)\cdot\pi/6 \quad \text{for } h \le a,$$

and
$$K_{A'}(h) = 0 \quad \text{for } h \ge a, \quad (4)$$

and similar expressions for $K_{B'}(h)$. According to this model, a and b are the largest length of a segment crossing respectively A' and B'. For a sphere, this length equals the diameter. $K_{A'}(0)$ and $K_{B'}(0)$ are equal to the volume of the individual features, respectively the average intra-grain pore A' and the average powder grain B'. As the two sets A and B are independently superposed to create X, one has according to Poisson's law:

$$1 = q_A + \exp\{-\theta_A \cdot K_{A'}(0)\} = q_B + \exp\{-\theta_B \cdot K_{B'}(0)\}. \quad (5)$$

Combining Eqs. 1, 2 and 3 leads to:

$$C_{X^c}(h) = (1-q_A)^2 \cdot \exp\{\theta_A \cdot K_{A'}(h)\} \cdot [1 - 2\cdot(1-q_B) + (1-q_B)^2 \cdot \exp\{\theta_B K_{B'}(h)\}]. \quad (6)$$

Using again Eq. 2, one gets the expression of the covariogram of X:

$$C_X(h) = 1 - 2\cdot q_B \cdot (1-q_A) + (1-q_A)^2 \cdot \exp\{\theta_A \cdot K_{A'}(h)\} \cdot [2q_B - 1 + (1-q_B)^2 \cdot \exp\{\theta_B \cdot K_{B'}(h)\}]. \quad (7)$$

The value of the covariogram of X at the origin h = 0 is:

$$C_X(0) = (1-q_B) + q_A q_B, \quad (8)$$

which is not the sum of the porosity values q_A and $(1-q_B)$ because of the superposition of the two sets A and B.

The best fit values of the four parameters, a, b, q_A and q_B were looked for by varying them in a quite large range. As the pores between the grains are much larger than the intra-grain voids, b should be of the order of the length over which the experimental covariogram decreases to attain its asymptote, i.e. 13 to 15 pixels. Also, the observation of the images in Fig. 2 shows that a should be about a few pixels (say between 2 and 5), and that the fraction of the small and large pores should be quite similar. The procedure followed was thus to set b to a given value (13, 14 or 15 pixels) and to calculate the corresponding $K_{B'}(0)$ value. The next step was to select q_B (0.85, 0.875 or 0.9) which gives θ_B by means of Eq. 5 when $K_{B'}(0)$ is known. Then, the value of q_A was estimated by means of Eq. 8 with $C_X(0)$ set at the

experimental value. Finally, a was systematically varied in between 2 and 5 pixels. For each set of the four parameters, the covariogram was calculated by Eq. 7 and compared to the experimental one. It was found that the agreement was highly sensitive to the selected values. In other words, estimating the four parameters appeared quite easy as the discrepancy between the calculated and experimental covariograms changed dramatically with any change of the model parameters. The following set of values was finally selected: b = 15 pixels, $q_B = 0.875$, a = 4 pixels and $1-q_A = 0.913$ (or equivalently $q_A = 0.087$). The comparison between the calculated and recorded covariograms is shown in Fig. 6 where it is seen that the model reproduces satisfactorily the experimental information.

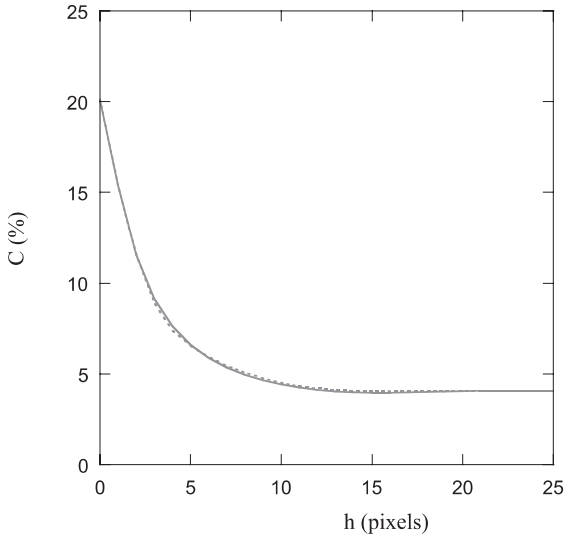

Fig. 6. *Comparison of the calculated (dotted line) and average experimental (solid line) covariograms C(h).*

From the above result, it could be decided that pores with largest size lower or equal to a = 4 pixels are intra-grain pores, whilst all other pores are inter-grain cavities. As mentioned above, the possibility of performing such a separation is based on the fact that it is very unlikely that small disconnected pores observed on the surface of the compact could be the visible part of large ones. Accordingly, the separation of the two populations could be made by an erosion-reconstruction procedure. In the present case, a linear element parallel to the long axis of the images was used. The result of such a separation is illustrated in Fig. 7 in the case of field 10. The same separation procedure was then applied to all the images (apart those excluded previously) and the covariograms were measured on the resulting images of intra and inter- pores. The average experimental covariograms are reported in Fig. 8 where have been also plotted the covariograms calculated with the best fit data listed above. It is seen that a satisfactory agreement is obtained with small discrepancies for intermediate values of h, namely in between 4 and 15 pixels. This may be due to the fact that grains, and thus intra-grain pores, are not single-sized as assumed.

To further check the appropriateness of the suggested separation, the calculated area distribution of the inter-grain pores obtained by linear erosion was compared to the experimental ones. It should be emphasised that such a comparison could not be made neither on the small pores nor on the whole porosity set because no theoretical expression is available for them. The experimental distribution was obtained as an average of the distributions measured on the images after exclusion of the pores with largest size smaller or equal to 4 pixels. The average curve is plotted with solid line in Fig. 9. The theoretical curve was calculated as (Jeulin, 1979):

$$Q(h) = (1-q_B)\cdot\exp[\theta_B\cdot h\cdot K'_B(0)] \qquad (9)$$

where $K'_{B'}(0)$ is the derivative of $K_{B'}$ for h equal to zero. It is seen in Fig. 9 that the calculated curve agrees satisfactorily with the experimental one, with again small discrepancies at intermediate sizes. As mentioned above, these discrepancies may come from the fact that the distribution of the grains may be not single sized as assumed for modelling. One point of particular interest is the fact that the size of the grain B' considered for the calculations is much smaller than the initial size of the powder grain. In fact, the powder when poured in the cylindrical die has a relative density below 0.1 while the final density is about 0.8 (Poquillon, 2002). The grains may thus be highly deformed during the compaction process, and this could explain that the size obtained by modeling is much smaller than the initial size of the grains.

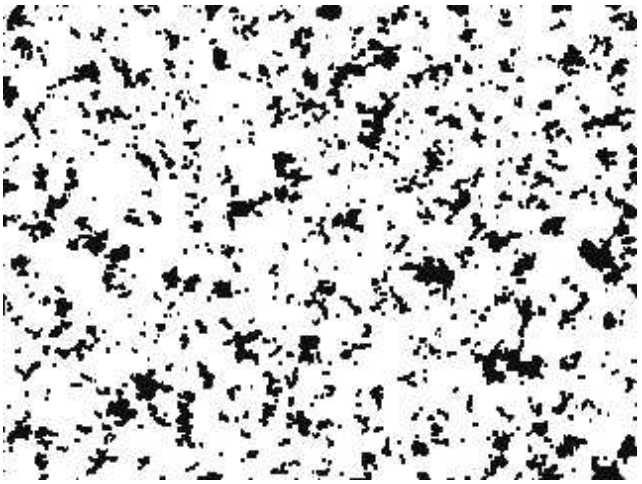

(a)

(b)

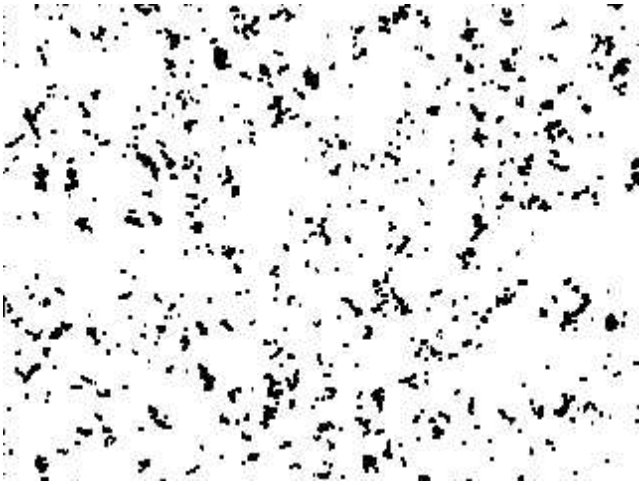

(c)

Fig. 7. *Initial image of field 10 (a) and images showing the large (b) and small (b) pores obtained by erosion/reconstruction of 4 pixels.*

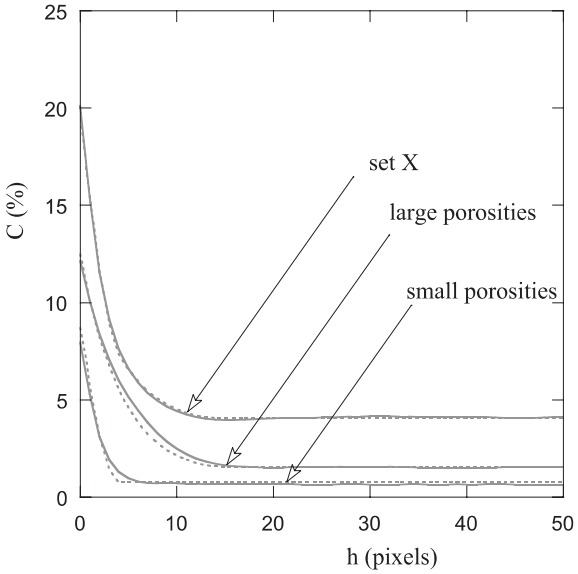

Fig. 8. *Comparison of the calculated (dotted lines) and experimental (solid lines) covariograms C(h) for the whole set X and for the two subsets, large and small pores.*

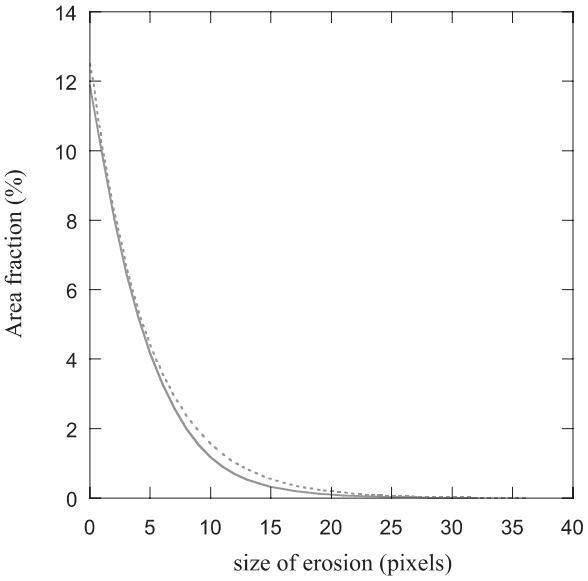

Fig. 9. *Comparison of the experimental area distribution of the inter-grain pores (solid curve) with the calculated one (dotted curve).*

CONCLUSION

In order to characterise microstructural features of green compacts made of spongy iron powders, images obtained from their surface have been analysed. Classical methods were not relevant to separate intra-particle porosity from inter-particle porosity in this material. The separation could be achieved by

comparing experimental covariograms with those obtained by modelling. For this purpose, the structure was described as the superposition of two sets of spherical elements randomly distributed, namely grains without internal cavities and intra-grain pores. The four parameters needed, two for each distribution, could be fitted satisfactorily on the experimental data. It is expected that this approach could help for further analysis of compacts made at various compaction pressures.

REFERENCES

Carles V, Alphonse P, Tailhades P, Rousset A (1999). Study of thermal decomposition of $Fe_2C_2O_4 \cdot 2H_2O$ under hydrogen. Thermochimica Acta 334:107-13.

Coster M, Chermant JL (1989). Précis d'analyse d'images. Les Presses du CNRS.

Jeulin D (1979). Morphologie mathématique et propriétés physiques des agglomérés de minerais de fer et du coke métallurgique. Thèse de docteur-ingénieur. School of Mines of Paris.

Özkan N, Briscoe BJ (1996). The surface topography of compacted agglomerates; a means to optimize compaction conditions. Powder Technology 86:201-7.

Poquillon D, Lemaitre J, Baco-Carles V, Tailhades P, Lacaze J (2002). Cold compaction of iron powders - Relations between powder morphology and mechanical properties. Part I: Powder preparation and compaction. Powder Technology 126:65-74.